Inter-seasonal compressed air energy storage using saline aquifers

Authors: Julien Mouli-Castillo*[a], Mark Wilkinson[a], Dimitri Mignard[b], Christopher McDermott[a], R. Stuart Haszeldine[a], Zoe K. Shipton[c]

[a] Grant Institute, School of GeoSciences, University of Edinburgh, West Mains Road, Edinburgh, EH9 3JW, UK

[b] Institute for Energy Systems, School of Engineering, University of Edinburgh, Mayfield Road, Edinburgh EH9 3DW, UK

[c] Department of Civil & Environmental Engineering, University of Strathclyde, Glasgow, G1 1XJ, UK

*Correspondence: Julien Mouli-Castillo, email: julien.moulicastillo@ed.ac.uk

Abstract

Meeting inter-seasonal fluctuations in electricity production or demand in a system dominated by renewable energy requires the cheap, reliable and accessible storage of energy on a scale that is currently challenging to achieve. Commercially mature compressed air energy storage (CAES) could be applied to porous rocks in sedimentary basins worldwide where legacy data from hydrocarbon exploration are available, and where geographically close to renewable energy sources. Here we present a modeling approach to predict the potential for CAES in porous rocks. By combining these with an extensive geological database we provide a regional assessment of this potential for the UK. We find the potential storage capacity is equivalent to approximately 160 % of the UK's electricity consumption for January and February 2017 (77 – 96 TWh), with a round-trip energy efficiency of 54 - 59 %. This UK storage potential is achievable at costs ranging from 0.42-4.71 US$ kWh^{-1}.

Meeting the target of limiting the increase in average global temperature to below 2°C by 2100 will require additional inherently variable renewable power sources, necessitating over 310 GW of grid-connected electricity storage worldwide by 2050[1]. However, power systems in which more than 80 % of the supply is generated from renewable sources cannot be balanced using daily and weekly storage alone[2] and will require inter-seasonal storage of a few months[2]. This is due, in part, to the

seasonal variation in electricity demand. For example in the UK, from 2012 to 2018, the winter demand was 25 % greater than the summer demand[3].

Worldwide, 165 GW of grid-connected storage capacity exists, 98 % of which is pumped hydro storage (PHS)[4] which is affected by water shortages, and social and geographical constraints[5,6]. Batteries are generally unsuitable for this task, due to high maintenance costs and limited discharge capacity[7]. Therefore there is a need to diversify the portfolio of grid-connected storage technologies to ensure energy security. More specifically, inter-seasonal storage will likely be a combination of PHS, CAES, and possibly geological hydrogen storage[8]. CAES is currently the only other commercially mature technology for this application[9]. It is therefore crucial to assess the inter-seasonal storage potential of CAES technology.

The two currently existing commercial CAES plants, Huntorf in Germany and McIntosh in the USA, store compressed air in underground caverns mined from salt[6,10]. Electricity is generated by expanding the air through a gas turbine fired with methane gas, known as "conventional" CAES[11] (Figure 1). Conventional CAES releases approximately 228 gCO_2 kWh^{-1}, less than the 388 gCO_2 kWh^{-1} reported for combined cycle gas turbines used in gas power plants[12]. CAES requires less land area per kWh of storage than PHS because the storage is underground[6]. Ongoing research on a fossil fuel-free CAES[13,14] could extend the use beyond the lifespan of fossil fuels.

If significant inter-seasonal storage is to be achieved, then safely storing hundreds of millions of cubic meters of air is needed. Porous media CAES (PM-CAES) would use porous rock formations called saline aquifers which contain saline (non-potable) water (Figure 1). The formations were originally deposited as sand-rich sediment in environments such as beaches, sandy deserts or rivers, and are often laterally extensive, extending for kilometers or tens of kilometers. Such aquifers are common worldwide[6] which offers greater total storage potential than mined salt caverns. In PM-CAES, compressed air would displace saline water within the μm-scale pores of the aquifers. One

competing use for this resource includes geological carbon storage, though some uses might be combined, e.g. PM-CAES with CO_2 as the cushion gas[15,16].

Here predictive models are used to estimate the potential of PM-CAES on a nationwide scale using the UK as a test case. The PM-CAES system is divided in three models, one for the store, another for the well, and one for the surface plant. Results from these three models are then used to determine the predictive models. The 77-96 TWh storage potential of offshore saline aquifers in the UK is then estimated using an established geological dataset[17].

Modelling PM-CAES

The PM-CAES system is described by three models (Figure 2 and Methods): first, a numerical geological porous rock store model (Figure 2a), from which pressure at the bottom of the well can be estimated throughout a PM-CAES cycle, using two-phase flow simulation[18] (summarized in Figure 3); second, an analytical well model linking the store to the surface facilities in order to estimate the pressure changes between the store and the surface[19] (Figure 2b); and third a numerical plant model composed of analytical models[6,20] for the compressor, turbine and combustor, to estimate the power consumption, power production, fuel consumption, and the process efficiency (Figure 2c). The simulations model 4 months of air injection at a rate of 7.5 kg s^{-1} followed by 3 months of storage, then 2 months of air production at 15 kg s^{-1}, finishing with 3 months idle. Comparable schedules are used worldwide in the underground seasonal storage of natural gas[21].

A sensitivity analysis of the porous rock store model varies the store's depth (i.e. the depth at which the air will accumulate due to its buoyancy), thickness, porosity and permeability within the ranges recommended for PM-CAES (Methods and Figure 2a). The store's thickness, porosity and permeability (both absolute value and vertical to horizontal ratio) have a negligible effect on the pressure variations in the store for the chosen cycling schedule[22]. This is due to the exceptionally good flow characteristics of the stores that were selected on the basis of geological characteristics for

PM-CAES recommended in the literature[23] (Table 1). The well pressure at the interface between the store and the overlying seal is proportional to the store's depth (adjusted $R^2 > 0.95$, Supplementary Figure 1). This relationship allows estimation of the well pressure at the store's top depth at any point during the cycle, including when the store is fully charged with air, and after 61 days of production.

Under correct operation, the cycling of pressure in porous reservoirs causes permanent deformation of the store which may stabilise after a number of years[24]. Under incorrect operation, the repeated pressure changes imposed on the rock can damage the store as a result of mechanical fatigue, fracturing of the rock or collapse of the well on itself[24,25]. To ensure no fracturing occurs during the store simulations, the storage pressure is fixed below the likely fracture pressure of the store and top seal whichever is the smallest. The pressure drop caused by the production of the compressed air is then modelled. In addition, an analytical well collapse model[26] is used to ensure borehole stability (see Methods and Supplementary Table 3). We found that a minimum store thickness of 50 m ensures the flow rate can be maintained during the 61 days of production without the well collapsing (Table 1). The integrity of the sealing rocks surrounding the store must also be considered. Approximately 70 % of the storage potential identified is located in stores with seals for which there is high confidence of a low risk of leakage, based on parameters independent from the injected gas[17]. The viability of PM-CAES cycles on a seasonal time scale has not been documented before, as most studies focus on the use of the technology for daily to weekly use[27-29]. Our models show that a PM-CAES store could meet flow rates needed for seasonal storage for two months.

The well model (Figure 2b) derived from Smith[20] and used in the hydrocarbon industry is validated using PM-CAES modelling studies from Oldenburg and Pan[27,30] (see Methods). The model shows that for PM-CAES, the pressure at which the gas exits the well increases with the store's depth because the pressure drop along the well is less than the increase of store pressure with depth. The

store depth is therefore limited to 4 km (Table 1) to prevent surface pressures exceeding ~250 bar, a likely maximum for commercial CAES turbines[31].

The plant model (Figure 2c) comprises eight plant simulations that use as inputs the pressure outputs from the store model sensitivity analysis, corrected for friction effects using the well model. Each simulation is performed using a different combination of turbine and compressor efficiencies for each input (TrainSet and TestSet sheets in Supplementary Data 1). We find that the power output corresponding to a well producing air at 15 kg s^{-1} varies from 4 to 11 MW (sample size = 736) ,which is slightly higher than the power output of most current offshore wind turbines. The process round-trip efficiency is a representative measure of how efficient PM-CAES is at storing electricity compared to other technologies (see Methods). The round-trip efficiencies from our study are 42 to 67 % (sample size = 736) which was within the 42 - 75 % range from the CAES literature[10,32-34]. This result agrees with the findings from previous daily PM-CAES modelling studies, that the losses from a porous rock store are manageable, and not significantly greater than that of air storage in salt caverns[27,30]. Our results show this conclusion holds true should PM-CAES be used for inter-seasonal storage.

In the final model workflow step (Figure 2d), predictive models are determined in the form of numerical relationships between the depth of the store, and both the power output (P_w) corresponding to a well, and the round-trip efficiency (η_{RT}) of the system. The potential of a store is determined by the pressure difference between atmospheric and mean pressure at the top of the well, since it is that pressure difference which determines the amount of energy input for the compressor and output for the turbine. The fluctuations in pressure inside the reservoir are used to refine the screening criteria. It is for this reason that the power output and round-trip efficiency are not correlated to the store's thickness, permeability and porosity. The following two multiple linear regressions predict the power output ($P << 0.001$, adjusted $R^2 = 0.9893$, sample size = 544) and round-trip efficiency ($P << 0.001$, adjusted $R^2 = 0.9529$, sample size = 544) respectively:

$$P_{\mathrm{w}} = -7.316 - 1.291\alpha + 3.439 \log D + 7.790\eta_{\mathrm{T}} \quad (1)$$

$$\eta_{\mathrm{RT}} = -23.23 - 1.078\alpha + 0.141\sqrt{D} + 46.46\eta_{\mathrm{T}} + 50.52\eta_{\mathrm{C}} \quad (2)$$

where P_{w} is the power output corresponding to a well delivering 15 kg s^{-1} of air to a gas turbine; D is the depth at the top of the store; η_{T} is the turbine polytropic efficiency, which is a measure of efficiency and is independent of the ratio of outlet to inlet turbine pressure, making the efficiency comparable between the different ratios of each simulation; η_{C}, is the compressor polytropic efficiency; α relates to the storage pressure in the store (pressure in the store when it is fully charged). The full regression statistics are reported in the Supplementary Table 1 and Supplementary Table 2, and the assumptions in the methods. The storage pressure varies between two end members: hydrostatic pressure caused by the column of fluid in the rocks above the store; and the fracture pressure above which the store will be damaged. Simulations are run for both end members. α is 1 when the storage pressure is set at the hydrostatic pressure and 0 when it is set at the fracture pressure, hence in practice $0 < \alpha \leq 1$. α can be used to linearly interpolate any storage pressure between the two end members modelled.

UK storage potential case study

The CO2 Stored dataset[17] contains characteristics of porous rock aquifers covering large areas of the UK Continental Shelf. This dataset was developed by a consortium of 10 public and private sector institutions using seismic, well data and literature, since 2009[17]. It contains (amongst others) the location, lithology, porosity, permeability, thickness and depth of offshore UK saline aquifers[17]. Although the database was compiled for CO_2 injection, the data required for assessment of PM-CAES is similar as both technologies involve fluid flow in the subsurface. There was no CO_2 specific manipulation of the CO2 Stored data, instead the database represents all of the relevant geological data that were available at the time of compilation. One limitation of the database is that geological units with less than 50 Mt of possible CO_2 storage were filtered out, so that some small units suitable for PM-CAES may be omitted. This is unlikely to affect the conclusions of this study,

as the units in the database approximately follow a power-law distribution, so that the greatest fraction of the total volume is found in a few formations, and not uniformly shared amongst many[17,35]. The database may also omit some units at depths less than 800 m, above which is unsuitable for geological carbon storage. However rocks (sediments) at such depth in the North Sea are poorly consolidated and are mechanically weak, therefore their PM-CAES potential is low as the potential pressure range is also low. Both the above omissions imply that the true PM-CAES potential of the UK offshore may be higher than the figures presented here.

The storage potential of UK prospective areas (Figure 4) is estimated using a Monte Carlo approach. The power output and efficiency of a large number of possible sites, and plants with the known range of properties, are computed. Here, the predictive models presented in equation (1) and (2) are substituted in the individual site simulations, with their simple algebraic form considerably reducing the simulation time. This approach would normally be very time consuming, even with modern computing power, mostly from the requirement for numerical simulations of many complex geological models of individual storage sites. The Monte Carlo simulation accounts for quantified uncertainties including: the error in the store pressure due to the linear approximation using depth; the heat capacity of air, which is assumed constant in the plant model; and the uncertainty in the aquifers' pore volume.

The results provide storage potential estimates of 77 to 96 TWh, (P_{10} to P_{90}; Figure 5) with an efficiency of 54 to 59 %. For comparison, estimates for CAES using onshore UK salt cavern stores suggest that a total of 8 TWh of storage could be achieved[36]. In addition, storage potential in areas of the Southern North Sea, East Irish Sea and Inner Moray Firth is colocated to windfarms (Figure 4). This could create valuable synergies between generation and storage.

Achieving the storage potential found requires 6,300 to 7,800 wells in total. Comparing this to the ~11,000 wells drilled in over 40 years by the UK North Sea hydrocarbon industry[37] highlights the

scale of the endeavour. Using an initial capital investment cost per well of approximately 16 - 59 million US$ (2018), and the operation schedule of this study, the levelised cost of generated stored electricity from offshore PM-CAES is 0.42 - 4.71 US$ kWh^{-1} (Table 2), about an order of magnitude more expensive than onshore PM-CAES and PHS on average (see Methods and Costings and Conversions sheets in Supplementary Data 1). Although the methods to calculate the cost of electricity storage vary, the variability of the reported costs account for enough uncertainty in parameters to be relevant for comparison. However, no reported values were found for inter-seasonal bulk grid connected electricity storage, and as such, care should be taken when comparing costs of technologies deployed for different purpose. We therefore recommend that PM-CAES projects should be initially developed onshore to improve the technology and reduce operational costs. We also recommend that further research be undertaken to quantify the costs of idle times as they are prominent in the case of inter-seasonal storage.

Discussion

Our results show that PM-CAES is a potentially viable large scale inter-seasonal electricity storage technology, crucial in power systems with over 80 % of their generation capacity provided by renewable energy sources. The small surface footprint of PM-CAES would benefit regions with limited land surface or water resources. This could make the technology attractive in populated regions with high energy demand.

Regarding the readiness of the approach for full scale implementation, CAES has been operating commercially for over 40 years, but is currently limited to daily energy storage given the limited volume capacities of the caverns used for storing the compressed air. Porous rock stores would enable the technology to operate over inter-seasonal timescales too. This would make PM-CAES a technology with multi-utility abilities. Versatile storage technologies able to provide a multitude of services to energy networks are likely to be of greater interest than technologies only able to provide a single service[38].

Areas for further study include chemical reactions that may occur due to the high oxygen content of air when injected into the generally reducing conditions of the subsurface. However, silicate-dominated sandstones are not very responsive to redox changes. Oil companies routinely inject seawater into reservoirs for pressure support, and these reservoirs continue to function. In the North Sea example, millions of tonnes of oxidizing seawater have been injected into the majority of oilfields, to maintain subsurface pressures. Sulphide minerals are likely to be the most reactive, and these do pose potential problems, with the possibility of formation damage, the generation of hydrogen sulphide and the loss of oxygen[6]. However, oxygen depletion of less than one-half percent by volume was observed in air stored for 6 months during field-test experiments[39]. For PM-CAES, mineral reactivity is likely to be site specific[40], and should be determined by experiments on a site-by-site basis, which is out of the scope of a regional assessment.

The role of organically mediated reactions, including the growth of biofilms, is also uncertain. Potentially problematic sulfur-oxidising bacteria are unlikely to survive[41] the compression process, which raises air temperatures to 100 – 200 °C in our models. In-situ organisms will be anaerobic bacteria and archea, however these are unlikely to survive an influx of toxic oxygen[42]. As with inorganic reactions, experiments on a site-by-site basis would reduce uncertainty, but are out of the scope of a regional assessment.

A further potential issue is the precipitation of salts around the borehole, due to the evaporation of the saline porewaters into the injected air. This effect will be most important in formations with very high porewater salinities, where sodium and potassium chlorides are the most likely precipitates, with volumetrically lesser carbonates including calcium carbonate. While even the most concentrated brine cannot contain sufficient solute to completely infill porosity upon drying, small precipitated crystals (‘fines’) could migrate and block the pore-throats that connect larger pores, substantially reducing permeability and hence fluid flow. Yet, only 3 % of the identified storage is in a formation containing brine close to saturation with a salinity of 28 percent by weight.

Seal stability, both mechanical and chemical, is also important, to ensure that the injected air remains within the reservoir. Seals in the study area are shales (deposited as muds) and evaporites including gypsum and halite, deposited by the evaporation of saline water in an arid climate. We have not modelled the effects of pressure cycling within the reservoir upon mechanical stability, but note that seals within gas storage facilities in porous rocks remain functional over the facility's lifetime. Potential chemical reactions, biotic or abiotic, will be similar to those within reservoirs, as above. A slow penetration of air into a seal for even a few meters may not be important, provided that it does not lead to catastrophic seal failure.

Conclusions

We developed a method to assess the PM-CAES potential in sedimentary basins with a worldwide distribution, specifically for inter-seasonal storage applications. This research finds that simple predictive models, with a clearly defined domain of applicability, can be used to scope PM-CAES potential. We report a walkthrough of how the predictive models can be used in conjunction with a Monte Carlo analysis and existing data to estimate ranges in PM-CAES potential on a regional scale. In the example of the UK North Sea, the energy storage potential of up to 96 TWh is sufficiently large to make seasonal storage (2 winter months) worthy of more detailed investigation. We also find that the efficiency of the PM-CAES system ranges from 42-67 %, and from 54-59 % for the UK regional assessment. Further research should focus on identifying sites within aquifers identified here, paying attention to the extent of both inorganic, and organically-mediated, chemical reactions within the reservoir, and possibly the overlying seal.

Methods

PM-CAES system modelling overview

The porous rock store model is a 2D radially symmetrical model developed to estimate the pressure fluctuation inside the store during 5 to 10 annual seasonal cycles, using the isothermal two-phase

flow (gas-liquid) simulator of the finite element code OpenGeoSys[18]. The isothermal solution is used as we assume that the injected air would be cooled after compression in order to reach the store at the store's temperature. Previous modelling studies have shown that the average temperature variation in the store is less than 3°C, except at the onset of injection where it is approximately 10°C[27]. This temperature drop has negligible influence on the well bottom pressure. Equations of state of air and water from the literature are used as described in ref.[22]. The capillary pressure – water saturation curve is derived from sandstone pore throat distribution data using the Laplace equation assuming a contact angle between the pore throat and the air-brine interface of 3° and an interfacial tension between the fluids of 72 dynes cm^{-1} [43]. The mass of the cushion gas, which is the air remaining in the store throughout the cycle, must be between 40 and 70 % of the total gas stored for most underground storage operations[21]. Therefore a mid-range value of 50 % is used. As shown in Figure 3, the outer boundary conditions for the volume of reservoir served by an individual well are set to no flow to simulate the effects of well interaction in an isotropic homogeneous porous rock store with a regular grid of wells. In a homogeneous porous rock store with a regular grid of wells, the pressure fluctuations caused by each well can be assumed equal. Therefore at points equidistant from two wells, the pressure gradients are equal (in opposite directions) and hence act as a no flow boundary. While the modelled circular units cannot be packed exactly together, with a hexagonal pattern in plan view there is only 10 % overlap between adjacent units, in the regions of the model with the lowest pressure changes. The model upper and lower boundaries are closed to flow to simulate the impermeable rock units sealing the store and preventing the air from escaping. The pressure outputs are sampled at the well mesh node corresponding to the store's shallowest depth. While the model includes simplifications, it provides a regional assessment of storage potential, without the task of individually modelling every potential storage site in an assessment area.

A sensitivity analysis is performed on the model to understand the system's response to changes in geological characteristics. In each scenario, the depth, thickness, porosity and permeability are varied

within the ranges subsequently described in the screening methodology. The ranges ensured no unrealistic parameter combination are modelled. The porosity and permeability are varied independently as, due to the permeability range spanning only one order of magnitude, a strong correlation is not expected. Pressure and temperature, which controls air density, are correlated with depth. Hence, for each scenario the model radius and mesh are adjusted to represent a volume of rock able to contain a volume of air corresponding to the desired mass of stored air – this corresponds to the developer of a PM-CAES site choosing the lateral spacing of wells. The air mass is taken as 158 million kg of air, which corresponds to the mass produced by a well with an air flow rate of 15 kg s^{-1} for 24 hours during 61 day, multiplied by two to account for the cushion gas. The production flow rate of air is selected as it is representative of natural gas flow rates from high quality reservoirs in the UK North Sea[44].

To ensure that the borehole would not be damaged by the pressure swings caused by the cycling of air we use a borehole collapse analytical model[26], with parameters tabulated in Supplementary Table 3. Four conservative assumptions are: 1) any fracture in the well is assumed to occur at the interface between the well and the porous rock. This is likely as this is the location of the greatest pressure variation. 2) The well collapse model does not account for reported strengthening effects caused by the heterogeneous stress fields around the well encountered in reality[45]. 3) No steel casing of the well is assumed, this would not be the case in reality 4) The store is assumed to be in a closed compartment within the porous rock aquifer. We therefore model the maximum pressure swings that might occur in the store to ensure that no fracturing or collapse of the well would occur. In this study the well is the point of weakness in the store model, hence if it can be shown to be stable, so is the remainder of the store. In reality the store might not be the weakest at the well-store interface, but equally the pressure variations are likely to be lower than the maximums modelled.

Only the scenarios in which no collapse of the borehole occurred are used as inputs to the well model and plant model. In addition, the results are filtered to exclude any outputs from simulations that have not reached at least 5 years of cycling within the 12 hours of computational run time allocated.

Well model

The pressure at the top of the well is estimated from equation (22) in Smith's[19] which we modify to account for unit conversions leading to equation (3) and verify against previous PM-CAES modelling studies[27,30]. The pressure predictions, using the rearranged equation (7), agreed to within 5 %.

$$Q = 61.75 \times \left(\frac{1.8\,T_0 - 459.67}{ZP_0(1.8T - 459.67)}\right)\sqrt{\frac{d^5}{f}\left(\frac{P_s^2 - e^S P_w^2}{e^S - 1}\right)} \tag{3}$$

$$\left(\frac{Q}{61.75} \times \frac{ZP_0(1.8\,T - 459.67)}{1.8\,T_0 - 459.67}\right)^2 = \frac{d^5}{f}\left(\frac{P_s^2 - e^S P_w^2}{e^S - 1}\right) \tag{4}$$

$$\frac{f(e^S - 1)}{d^5} \times \left(\frac{QZP_0(1.8\,T - 459.67)}{61.75\,(1.8\,T_0 - 459.67}\right)^2 = P_s^2 - e^S P_w^2 \tag{5}$$

$$e^S P_w^2 = P_s^2 - \frac{f(e^S - 1)}{d^5} \times \left(\frac{QZP_0(1.8\,T - 459.67)}{61.75\,(1.8\,T_0 - 459.67}\right)^2 \tag{6}$$

$$P_w = \sqrt{\frac{{P_s}^2 - \left(\frac{QZ(1.8\,T - 459.67)P_0}{61.75\,(1.8\,T_0 - 459.67)}\right)^2 \frac{f(e^S - 1)}{d^5}}{e^S}} \tag{7}$$

where Q is the volumetric flow rate in m^3s^{-1}; Z is the dimensionless effective compressibility factor of the gas; T is the effective flowing temperature of the gas (K); f is the dimensionless friction coefficient; d is the inside diameter of the well (m); P_s is the upstream pressure with respect to direction of the flow (bar); P_w is the downstream pressure with respect to direction of the flow (bar); S is the exponent defined by $0.123045GL/[(1.8T-459.67)Z]$; G is the specific gravity of the gas, which is unity for air; L is the length of the well with respect to flow direction in meters (negative

during injection); T_0 and P_0 are the atmospheric temperature and pressure respectively (P_0 = 1 bar and T_0 = 289 K).

Plant model

The power output and efficiency are determined using a plant model. The pressure at the top of the well is assumed to be the inlet pressure for the turbine, assuming that the turbine would be located directly above the well. Indeed, the pressure drop that would be caused by sending the air to an onshore plant would be too great for the system to be economically viable[22]. In addition, turbines and compressors have been used successfully on offshore platforms by the hydrocarbon industry for many decades[46].

The work output from the turbine is estimated using equation (8), which is adopted from CAES literature[6,20]:

$$W_t = s\frac{kRT_{\text{in}}}{k-1}\left[\left(\frac{P_{\text{out}}}{P_{\text{in}}}\right)^{\eta_{\text{pol}}(k-1)/sk} - 1\right] \tag{8}$$

The work input to the compressor is estimated using:

$$W_c = s\frac{kRT_{\text{in}}}{k-1}\left[\left(\frac{P_{\text{out}}}{P_{\text{in}}}\right)^{k-1/\eta_{\text{pol}}sk} - 1\right] \tag{9}$$

where W is the specific work output from the device; s is the number of stages of the device; k is the specific heat capacity ratio, assumed to be 1.4 for air; R is the gas constant; T_{in} is the inlet temperature; P denotes the pressure and the subscripts “in” and “out” whether it is at the inlet or outlet of the device; and η_{pol} is the polytropic efficiency of the device.

The power (P) input and outputs can then be calculated using the mass flow rate of air, q, through either the compressor or turbine:

$$P = qW \tag{10}$$

The amount of energy, E, necessary for the compression of air and recoverable from its expansion is calculated using:

$$E = \sum_{n=1}^{N} P_n(t_n - t_{n-1}) \tag{11}$$

where N is the total number of output from the numerical model of the store.

The amount of heat, Q_{in}, required to re-heat the air prior to expansion is calculated using equation (12). The inlet temperature of the combustion chamber is determined accounting for heat losses from the well to the surrounding rock[47].

$$Q_{\text{in}} = m_{\text{CH}_4} \times LHV_{\text{CH}_4} \times \eta_{\text{comb}} \tag{12}$$

where m_{CH4} is the mass flow rate of methane burned every second to heat the air from atmospheric temperature to the turbine inlet temperature. The turbine inlet temperature is assumed to be 400 K greater than the inlet temperature to the combustion chamber, which is within the inlet temperature range for the Huntorf and McIntosh CAES plants[11]. LHV_{CH4} is the amount of energy produced by the complete combustion of one kilogram of methane, and η_{comb} is the efficiency of the combustion. This efficiency is taken as 93 % after calibrating our model using data from the Huntorf CAES plant[51].

The round-trip efficiency of the system is then calculated using:

$$\eta_{\text{RT}} = \frac{E_{\text{out}}}{E_{\text{in}} + Q_{\text{in}}\eta_{\text{sys}}} \tag{13}$$

where E_{out} is the total energy discharged by the PM-CAES plant; E_{in} the energy supplied to the compressor; Q_{in} the amount of heat added to the system as natural gas; η_{sys} = 0.476 the typical efficiency of converting energy from natural gas to electricity in a conventional CAES plant[6]. This conversion is needed to account for the different energy types (electrical and thermal) used as inputs and it makes the measure of round-trip efficiency comparable to that of other types of plants[6].

A sensitivity analysis is performed for the plant model. The polytropic efficiency of the compressor and turbines are uniformly sampled from a range of 66 to 88 %[11]. These efficiencies assume a generator and motor with an efficiency of 95 %[14]. While this procedure is useful for broad, nation-scale scoping purpose, more detailed calculations would be required for an individual plant. The number of compression stages was selected to ensure the compression pressure ratio was as close as possible to 3:1 without exceeding that value, a value used in previous CAES studies[48].

Power and energy predictive models

The predictive models are developed using the 736 power outputs and round-trip efficiencies from the PM-CAES system sensitivity analysis presented above. Multiple variable regressions are performed on the data. The data are divided into two sets, a training set, encompassing 74 % of the data, on which the regressions are performed, and a test set, encompassing the remaining 26 %, used to verify the predictive capabilities of the regressions. Store depth and turbine power output have an approximately logarithmic relationship; store depth and round-trip efficiency have a power law relationship. The data and regression statistics are tabulated in the Supplementary Table 1, Supplementary Table 2 and the TrainSet sheet in Supplementary Data 1.

UK storage potential

The predictive models are applied to a dataset of UK offshore aquifers (CO2 Stored database described in the main text)[17]. CO2 Stored used all available data (MW and RSH were part of the original team). Hundreds of primary sources were used, some of which are confidential or subject to stringent license conditions. Unfortunately, there is no publication that well describes the database. The primary sources of information are however indicated in the database itself, but subject to licensing terms. There are four key steps to the procedure. First, screening criteria are defined for PM-CAES stores based on published criteria ranges modified for state of the art CAES turbine technology (Table 1). Site specific criteria which are unfeasible to estimate using formation

characteristics are not used in the screening process (e.g. a minimum seal slope). Second, the database is screened using the criteria. Third, the volume of pore space within each of the aquifers in the database in which air can be stored is determined. Finally, using the depth and pore volumes from the screened dataset as input, a Monte Carlo analysis is performed by randomly sampling turbomachinery parameters to determine power output and round-trip efficiency. More details on the case study methods can be found in ref.[22].

Screening of UK dataset.

The aquifers from the CO2 Stored dataset, whose characteristics indicate they are likely to contain rocks suitable for PM-CAES, are identified based on their shallowest depth, porosity, permeability, thickness, lithology, and the presence of a geological trap to contain stored air and absence of features impeding the flow of air (mineral cement, heterogeneity of the rock mass). A geological trap is defined by a porous reservoir with an impermeable overlying seal plus lateral seals to flow. Such lateral seals could be provided by doming of the top seal, lateral changes in rock type to lower porosity units, or the presence of impermeable faults. In the following text we refer to this as trap geometry.

The screening procedure has five steps. First we remove all the entries for which no data is available for one or more of the screening criteria. Second, aquifers with 1 or more parameters outwith the allowable ranges of the screening criteria are rejected (Table 1). Third, aquifers are rejected if geological problems (e.g. heterogeneity, mineral cement, fractured seals, and overpressure) are identified from the literature. Fourth, the entries are divided into 3 categories: type 1 are entire single aquifer units; type 2 are subsets of single aquifers which are subdivided in the database into pressure compartments. These pressure cells are usually much larger than individual hydrocarbon fields or traps; type 3 are individual storage sites, i.e. locations within an aquifer defined usually as single geological traps. When an aquifer has entries of both type 1 and type 3, the type 3 are used.

Type 1 entries are subdivided using criteria identified in the literature[49-53], to make them into type 2 entries. Parameters used for sub-division include burial depth; thickness; permeability and the proportion of useable reservoir within the total thickness ('net-to-gross ratio'). The superposition of the parameters in ArcMap® GIS software enables the calculation of the pore volume of the sub-divided portions of the aquifers (Supplementary Figure 2).

The calculation of pore volume fraction of selected aquifers usable for storage is here described. Only a fraction of the pore volume of an aquifer, referred to as the usable pore volume (V_{usable}, equation (14), can actually be used for air storage. The usable pore volume is the pore volume within geological traps potentially capable of retaining fluids (e.g. a dome of porous rock overlain by impermeable seal). It excludes geological traps containing hydrocarbons or defects such as a fractured seals.

$$V_{\text{usable}} = V_{\text{traps}} \times \eta_{\text{usable}} \tag{14}$$

where V_{traps} is the pore volume contained in all the areas of the aquifer contained within a geological trap capable of retaining fluids (e.g. air, CO_2 or hydrocarbons), η_{usable} is the fraction of geological traps usable for air storage.

For Type 2 aquifers, this volume is estimated using equation (15).

$$V_{\text{traps}} = {}^{V_{\text{h}}}/_{\eta_{\text{h}}} \tag{15}$$

where V_{h} is the total pore volume of all the geological traps that contain hydrocarbons within an aquifer (a known value), and η_{h} the ratio of V_{h} to the total pore volume within geological traps.

The average success rate of hydrocarbon exploration wells from 1963 to 2002 is 30 %[54,55]. Assuming exploration wells are targeted at traps within an aquifer which can be identified by offshore imaging technics, we can use this value as η_{h}. The pore volume of geological traps exploited for hydrocarbons (V_{h}) is calculated from the hydrocarbon volumes originally in place in all the

hydrocarbon fields within the aquifers offering potential for PM-CAES (sample size = 44, Supplementary Table 4).

The fifth and final step is to estimate how many of those traps would be suitable for PM-CAES. The study of 382 hydrocarbon wells from Xia and Wilkinson[55] proposes that 49 %±8 of the traps in an aquifer can be successfully exploited for CO_2 storage. Because the prerequisites for CO_2 storage sites and compressed air storage sites are comparable, we assume that for CAES in aquifers, the only suitable traps would be the ones which could be successfully exploited as CO_2 stores but do not contain hydrocarbons. In that case, η_{usable} is equal to 19 % of the overall geological traps, see Supplementary Figure 4.

The storage efficiency of type 2 aquifers is given by equation (16).

$$\eta_{\text{storage}} = \frac{V_{\text{usable}}}{V_{\text{dataset,Type2}}} \tag{16}$$

For Type 3 aquifers, for which the geological trap pore volume, V_{traps}, is provided in the database, the efficiency is given by equation (17).

$$\eta_{\text{storage}} = \eta_{\text{usable}} \tag{17}$$

Monte Carlo Simulation.

A Monte Carlo simulation of the population of screened aquifers is performed to estimate the storage power and energy capacity achievable over two months of storage. There are nine steps of the algorithm used to perform each realization of the simulation. First, selecting a storage pressure using the alpha parameter and the hydrostatic pressure at the depth of the geological store. Alpha was varied between 0 which represents a storage pressure closer to fracture pressure, and 1 for one close to hydrostatic pressure. Second, selecting turbomachinery efficiencies from uniform distributions. Third, the power output per well is calculated using equation (1). Fourth, the power output is varied randomly by up to ±3 % from the calculated value to account for the uncertainty caused by using a

constant specific heat for air in equation (8). Fifth, the air mass which could be stored is the product of the usable pore volume (calculated using the storage efficiency $\eta_{storage}$ corresponding to the aquifer type), the gas density and the fraction of the pore space occupied by air within a PM-CAES store (i.e. the gas saturation). An arithmetic average of 47 % for the gas saturation is calculated from ten numerical store models representative of the parameter space in Table 1. Sixth, the number of wells needed is calculated as the mass of air per well divided by twice the amount of air which would be extracted over 2 months at a rate of 15 kg s^{-1}, equating to 158 million kg of air. The amount of air is doubled to account for the cushion gas requirement, which is the amount of air which remains in the store throughout the cycle. Seventh, the power output per aquifer is computed as the number of wells multiplied by the power output per well. Eighth, the energy storage potential is determined as the power output per well multiplied by the duration of the production period. Finally, the total power and energy storage potential per aquifer are achieved by a sum of all the entries' values for each aquifer.

Three simulations of 50,000 realisations are performed resulting in a maximum difference between simulations of ± 0.1 GW for power capacity estimates and ± 0.1 TWh for energy capacity estimates. The estimates of each individual formation are reported in Supplementary Figure 3.

Cost estimates

Cost estimates are calculated using the net present value (NPV), for 2015; of the cost of offshore wells[56]; transmission costs[57]; turbine[58] and compressor[58] initial capital costs and operation and maintenance costs (O&M); natural gas fuel costs; and electricity cost to power the compressor[59]. A 10 % discount rate is assumed in the calculations. Decommissioning costs are also accounted for[56]. The initial capital cost for the turbine and compressor are estimated using the results from a study on CAES sites on islands[58]. Its heat rate is assumed at 4,000 Btu kWh^{-1} which is equivalent to the McIntosh plant[59].

The levelised cost of generated stored electricity (LCOE) for the PM-CAES system is calculated as the sum of the discounted costs per year over the annual energy production from the storage facility, based on ref. [56]:

$$LCOE = \frac{\sum_{t=1}^{n} \frac{W_t + T_t + C_t + M_t + F_t + S_t + D_t}{(1+r)^t}}{\sum_{t=1}^{n} \frac{E_t}{(1+r)^t}} \quad (18)$$

where W_t is the well initial investment expenditure; T_t and C_t the turbine and compressor initial investment, respectively; M_t, the fixed operation and maintenance expenditures; F_t and S_t the fuel and compressor electricity supply expenditure, respectively. The subscript t denotes the year in which the expenditure occurs. E_t is the electrical energy generated by the CAES plant. r is the discount rate and n the lifetime of the CAES project. The metric in equation (18) is commonly used to compare storage technologies amongst themselves, as well as against other electricity generating technologies, as demonstrated by the references used in Table 2. The cycling schedule from this study is equivalent to a capacity factor of 0.17. The average power output from the turbine and input to the compressor over the generation and charging times is used, respectively.

Equation (18) is used to determine the costs of a few test cases. Those test cases include a best case, mid-range, and worst-case scenario (Supplementary Tables 6, 7 and 8), as well as tests cases using cost parameters derived from analog costing studies for CO_2 injection in offshore porous rocks, and test cases for which the power storage target is set using areas with storage potential identified in this study (Costings sheet in Supplementary Data 1). The best case scenario discount factor is of 6%[9]. This method allows for a LCOE range to be established (Table 2), and verifies it using test cases anchored in analog studies and expected storage potential.

The conversion to 2018 US$ of the reported costs from Table 2 are achieved using the currency exchange rates from the International Monetary Fund to convert to US dollars[60], and adjusted for inflation[61] (see Conversions sheet in Supplementary Data 1).

References

1. Lott, M. C. & Kim, S.-I. *Technology Roadmap Energy storage*. *International Energy Agency* (2014). Accessed 22nd November 2018 at: https://www.iea.org/publications/freepublications/publication/TechnologyRoadmapEnergystorage.pdf

2. Elliott, D. A balancing act for renewables. *Nat. Energy* **1,** 15003 (2016).

3. GridWatchUK. GridWatchUK. (2018). Accessed 22nd November 2018 at: http://www.gridwatch.templar.co.uk/index.php.

4. USDOE. Global Energy Storage Database. *US Department of Energy* (2017). Accessed 22nd November 2018 at: http://www.energystorageexchange.org/.

5. Rosenberg, D. M., Bodaly, R. a. & Usher, P. J. Environmental and social impacts of large scale hydro-electric development: Who is listening? *Glob. Environ. Chang.* **5,** 127–148 (1995).

6. Succar, S. & Williams, R. *Compressed Air Energy Storage : Theory, Resources, And Applications For Wind Power*. (2008). Accessed 22nd November 2018 https://acee.princeton.edu/wp-content/uploads/2016/10/SuccarWilliams_PEI_CAES_2008April8.pdf

7. Chen, H., Ngoc, T., Yang, W., Tan, C. & Li, Y. Progress in electrical energy storage system : A critical review. *Prog. Nat. Sci.* **19,** 291–312 (2009).

8. Amid, A., Mignard, D. & Wilkinson, M. Seasonal storage of hydrogen in a depleted natural gas reservoir. *Int. J. Hydrogen Energy* **41,** 5549–5558 (2016).

9. Zakeri, B. & Syri, S. Electrical energy storage systems: A comparative life cycle cost analysis. *Renew. Sustain. Energy Rev.* **42,** 569–596 (2015).

10. Crotogino, F., Mohmeyer, K.-U. & Scharf, R. Huntorf CAES : More than 20 Years of Successful Operation. in *Solution Mining Research Institute (SMRI) Conference* 1–7 (2001). Accessed 15th of October 2018 at: http://www.fze.uni-saarland.de/AKE_Archiv/AKE2003H/AKE2003H_Vortraege/AKE2003H03c_Crotogino_ea_HuntorfCAES_CompressedAirEnergyStorage.pdf

11. Kaiser, F. & Efzn, E. N. Steady State Analyse of existing Compressed Air Energy Storage Plants Thermodynamic Cycle modeled with Engineering Equation Solver. in *Power and Energy Student Summit (PESS)* (2015).

12. Mason, J. E. & Archer, C. L. Baseload electricity from wind via compressed air energy storage (CAES). *Renew. Sustain. Energy Rev.* **16,** 1099–1109 (2012).

13. Helsingen, E. M. Adiabatic compressed air energy storage. (Norwegian University of Science and Technology, 2015). Accessed on the 15th of October 2018 at : https://brage.bibsys.no/xmlui/handle/11250/2350057

14. Kim, Y. M., Lee, J. H., Kim, S. J. & Favrat, D. Potential and evolution of compressed air energy storage: Energy and exergy analyses. *Entropy* **14,** 1501–1521 (2012).

15. Oldenburg, C. M. & Pan, L. Utilization of CO2 as cushion gas for porous media compressed air energy storage. *Greenh. Gases Sci. Technol.* **3,** 124–135 (2013).

16. Buscheck, T. A. *et al.* Multifluid geo-energy systems: Using geologic CO2storage for geothermal energy production and grid-scale energy storage in sedimentary basins. *Geosphere* **12,** 678–696 (2016).

17. Bentham, M., Mallows, T., Lowndes, J. & Green, A. CO2 STORage Evaluation Database (CO2 Stored). The UK's online storage atlas. *Energy Procedia* **63,** 5103–5113 (2014).

18. Kolditz, O. *et al.* OpenGeoSys: An open-source initiative for numerical simulation of thermo-

hydro-mechanical/chemical (THM/C) processes in porous media. *Environ. Earth Sci.* **67,** 589–599 (2012).

19. Smith, R. V. Determining friction factors for measuring productivity of gas wells. *Pet. Trans.* **189,** 73–82 (1950).

20. Barbour, E., Mignard, D., Ding, Y. & Li, Y. Adiabatic Compressed Air Energy Storage with packed bed thermal energy storage. *Appl. Energy* **155,** 804–815 (2015).

21. Flanigan, O. Chapter 6: *Characteristics of underground storage*. In *Underground Gas Storage Facilities: Design and Implementation* (1995). pp. 54–67. Houston, London, Paris, Zurich, Tokyo: Golf Publishing Company. http://doi.org/http://dx.doi.org/10.1016/B978-088415204-0/50006-6

22. Mouli-Castillo, J. PhD Thesis: Assessing the potential for Compressed Air Energy Storage using the offshore UK saline aquifer resource. (The University of Edinburgh, 2018). Accessed on the 22nd of November 2018 at: https://www.era.lib.ed.ac.uk/bitstream/handle/1842/31051/Mouli-Castillo2018.pdf?

23. Allen, R. D., Doherty, T. J., Erikson, R. L. & Wiles, L. E. *Factors affecting storage of compressed air in porous-rock reservoirs*. (1983). Accessed on the 15th of October 2018 at: https://www.osti.gov/biblio/6270908

24. Castelletto, N. *et al.* 3D geomechanics in UGS projects: a comprehensive study in northern Italy. in *44th American Rock Mechanics Association Symposium* (2010). ARMA-10-185, Accessed on the 22nd of November 2018 at: https://site.tre-altamira.com/wp-content/uploads/2010_3D_geomechanics_in_UGS_projects_comprehensive_study_in_northern_Italy.pdf

25. Watson, K. & Jones, C. Cyclic Loading of a Rock Mass for Underground Gas Storage

Applications. in *SIMULIA Customer Conference* 1–9 (2010). Accessed on the 22nd of November 2018 at: http://www.simulia.com/download/scc-papers/Energy/cyclic-loading-rock-mass-underground-gas-storage-2010-F.pdf

26. Aadnoy, B. S. & Kaarstad, E. History Model for Sand Production During Depletion. in *SPE EUROPEC/EAGE Annual Conference and Exhibition* 14–17 (2010).

27. Oldenburg, C. M. & Pan, L. Porous Media Compressed-Air Energy Storage (PM-CAES): Theory and Simulation of the Coupled Wellbore–Reservoir System. *Transp. Porous Media* **97,** 201–221 (2013).

28. Allen, R. D. & Gutknecht, P. J. *Porous Media Experience Applicable to Field Evaluation for Compressed Air Energy Storage*. *Pacific Northwest Laboratory* (1980). Accessed on the 22nd of November 2018 at: https://www.osti.gov/servlets/purl/5319221

29. Maton, J.-P., Zhao, L. & Brouwer, J. Dynamic modeling of compressed gas energy storage to complement renewable wind power intermittency. *Int. J. Hydrogen Energy* **38,** 7867–7880 (2013).

30. Pan, L. & Oldenburg, C. M. Rigorous process simulation of compressed air energy storage (CAES) in porous media systems. in *Computational Models for CO2 Geo-sequestration & Compressed Air Energy Storage* (eds. Al-Khoury, R. & Bundschuh, J.) 479–498 (2014).

31. Dresser-Rand. SMARTCAES®. (2017). Accessed on the 22nd of November 2018 at: http://www.dresser-rand.co.uk/products-solutions/systems-solutions/compressed-air-energy-storage-solutions/.

32. Grazzini, G. & Milazzo, A. A thermodynamic analysis of multistage adiabatic CAES. *Proc. IEEE* **100,** 461–472 (2012).

33. Xing, L. & Jihong, W. *Overview of Current Development on Compressed Air Energy Storage.*

EERA Technical Report. (2013). Accessed on the 22nd of November 2018 at: https://www.eera-set.eu/wp-content/uploads/Overview-of-Current-Development-on-Compressed-Air-Energy-Storage_EERA-report-2013.pdf

34. Liu, W. *et al.* Analysis and Optimization of a Compressed Air Energy Storage—Combined Cycle System. *Entropy* **16,** 3103–3120 (2014). Accessed on the 15th of October 2018 at: https://www.eera-set.eu/wp-content/uploads/Overview-of-Current-Development-on-Compressed-Air-Energy-Storage_EERA-report-2013.pdf

35. Wilkinson, M. *et al.* Defining simple and comprehensive assessment units for CO2 storage in saline formations beneath the UK North Sea and continental shelf. *Energy Procedia* **4,** 4865–4872 (2011).

36. Evans, D., Parkes, D., Bgs, J. B. & Nottingham, S. G. Initial Studies to Derive Estimates of Potential UK Salt Cavern Volumes and Exergy Storage (CAES). (2016). Accessed on the 15th of October 2018 at: http://energysuperstore.org/esrn/wp-content/uploads/2017/01/UKES2016_David-Evans-Initial-Studies-to-Derive-Estimates-of-Potential-UK-Salt-Cavern-Volumes-and-Exergy-Storage.pdf

37. Oil & Gas Authority. Well data. (2017). Accessed on the 9th October 2017at: https://www.ogauthority.co.uk/data-centre/data-downloads-and-publications/well-data/.

38. Kittner, N., Lill, F. & Kammen, D. M. Energy storage deployment and innovation for the clean energy transition. *Nat. Energy* **2,** 17125 (2017).

39. Kushnir, R., Ullmann, A. & Dayan, A. Thermodynamic and hydrodynamic response of compressed air energy storage reservoirs: a review. *Rev. Chem. Eng.* **28,** 123–148 (2012).

40. Wang, B. & Bauer, S. Pressure response of large-scale compressed air energy storage in porous formations. *Energy Procedia* **125,** 588–595 (2017).

41. Niemela, S. I., Sivela, C., Luoma, T. & Tuovinen, O. H. Maximum temperature limits for acidophilic, mesophilic bacteria in biological leaching systems. *Appl. Environ. Microbiol.* **60,** 3444–3446 (1994).

42. Madigan, M. T., Martinko, J. M., Dunlap, P. V. & Clark, D. P. *Brock biology of microorganisms*. (Int. Microbiol., 2008).

43. Kalantarian, A., David, R., Chen, J. & Neumann, A. W. Simultaneous measurement of contact angle and surface tension using axisymmetric drop-shape analysis-no apex (ADSA-NA). *Langmuir* **27,** 3485–3495 (2011).

44. BERR. BERR Well Production. (2007). Accessed on the 25th August 2017 at: https://itportal.decc.gov.uk/information/wells/pprs/Well_production_offshore_gas_fields/offshore_gas_fields_by_well/offshore_gas_fields_by_well.htm

45. Al-ajmi, A. M. & Zimmerman, R. W. Stability analysis of vertical boreholes using the Mogi – Coulomb failure criterion. *Int. J. Rock Mech. Min. Sci.* **43,** 1200–1211 (2006).

46. Wall, M., Lee, R. & Frost, S. *Offshore gas turbines (and major driven equipment) integrity and inspection guidance notes*. *Prepared by ESR Technology Ltd for the Health and Safety Executive* (2006). Research Report 430. Accessed on the 22nd of November 2018 at: http://www.hse.gov.uk/research/rrpdf/rr430.pdf

47. Kutun, K., Tureyen, O. & Satman, A. Analysis of wellhead production temperature derivatives. in *40th Workshop on Geothermal Reservoir Engineering, Stanford University* 26-28 (2015). SGP-TR-204. Accessed on the 22nd of November 2018 at: http://docplayer.net/49385718-Analysis-of-wellhead-production-temperature-derivatives.html

48. Liu, W. *et al.* Performance Analysis of a Coal-Fired External Combustion Compressed Air Energy Storage System. *Entropy* **16,** 5935–5953 (2014).

49. Ahmadi, Z., Sawyers, M., Kenyon-Roberts, S., Stanworth, B., Kugler, K., Kristensen, J., & Fugelli, E. (2003). Paleocene. In D. Evans, C. Graham, A. Armour, & P. Bathurst (Eds.), The Millennium Atlas: Petroleum Geology Of The Central And Northern North Sea: Geological Society (pp. 253–259). London: The Geological Society of London. ISBN: 186239119X, 9781862391192

50. Knox, R. W. & Holloway, S. Paleogene of the central and northern North Sea. in *Lithostratigraphic Nomenclature of the UK North Sea* (eds. Knox, R. W. & Cordey, W. G.) (1992).

51. Mudge, D. C. & Bujak, J. P. An integrated stratigraphy for the Paleocene and Eocene of the North Sea. *Geol. Soc. London, Spec. Publ.* **101,** 91–113 (1996).

52. Kilhams, B. A. PhD Thesis: An Integrated Characterisation of the Paleocene Submarine Fan Systems (Lista and Maureen Formations) in the Central Graben of the North Sea. (University of Aberdeen, 2011).

53. Kilhams, B., Hartley, A., Huuse, M. & Davis, C. Characterizing the Paleocene turbidites of the North Sea: the Mey Sandstone Member, Lista Formation, UK Central Graben. *Pet. Geosci.* **18,** 337–354 (2012).

54. Munns, J. W., Gray, J. C., Stoker, S. J., Andrews, I. J. & Cameron, T. D. J. The remaining hydrocarbon potential of the UK Continental Shelf. in *Petroleum Geology: North-West Europe and Global Perspectives — Proceedings of the 6th Petroleum Geology Conference, 41–54. Petroleum Geology Conferences Ltd.* (ed. Doré, A. G. & Vining, B. A.) (Geological Society, 2005). https://doi.org/10.1144/0060041

55. Xia, C. & Wilkinson, M. Quantifying the geological risk of drilling a borehole for CO2 storage. *Int. J. Greenh. Gas Control* **63,** 272–280 (2017).

56. Pale Blue Dot Energy. *Progressing development of the UK's Strategic Carbon Dioxide Storage Resource: A Summary of Results from the Strategic UK CO2 Storage Appraisal Project*. (2016). Accessed on the 15th of October 2018 at: https://www.eti.co.uk/programmes/carbon-capture-storage/strategic-uk-ccs-storage-appraisal.

57. Offsore Wind Programme Board. *Transmission Costs for Offshore Wind Final Report April 2016*. (2016). Accessed on the 15th of October 2018 at: https://ore.catapult.org.uk/app/uploads/2018/02/Transmission-Costs-for-Offshore-Wind.pdf

58. Mignard, D. Estimating the capital costs of energy storage technologies for levelling the output of renewable energy sources. *Int. J. Environ. Stud.* **71,** 796–803 (2014).

59. Steward, D., Saur, G., Penev, M. & Ramsden, T. *Lifecycle Cost Analysis of Hydrogen Versus Other Technologies for Electrical Energy Storage*. (2009). Accessed on the 15th of October 2018 at: https://www.nrel.gov/docs/fy10osti/46719.pdf

60. IMF. Exchange Rate Archives by Month. *Data and Statistics* (2018). Available at: https://www.imf.org/external/np/fin/data/param_rms_mth.aspx. (Accessed: 10th October 2018)

61. Labor, U. S. D. of. Databases, Tables & Calculators by Subject: CPI Inflation Calculator. (2018). Accessed on the 15th of October 2018 at: https://www.bls.gov/data/inflation_calculator.htm

62. Obi, M., Jensen, S. M., Ferris, J. B. & Bass, R. B. Calculation of levelized costs of electricity for various electrical energy storage systems. *Renew. Sustain. Energy Rev.* **67,** 908–920 (2017).

63. McGrail, B. P. *et al. Techno-economic Performance Evaluation of Compressed Air Energy Storage in the Pacific Northwest*. (2013). PNNL-22235. Accessed on the 22nd of November

2018 at: https://caes.pnnl.gov/pdf/PNNL-22235.pdf

64. Eckroad, S. & Gyuk, I. EPRI-DOE handbook of energy storage for transmission & distribution applications. *Electr. Power Res. Institute, Inc* (2003). Report number 1001834. Accessed on the 22nd of November 2018 at: www.sandia.gov/ess/publications/ESHB%201001834%20reduced%20size.pdf

Acknowledgments

This work has been funded by the Engineering and Physical Science Research Council (EPSRC) of the UK, and by the Energy Technology Partnership. The authors would like to thank E.V. Hipkins for her proof reading of the draft, as well as the Geofluids research group from the University of Edinburgh for their suggestions.

Data Availability

The data used to determine the predictive models are provided in the TrainSet and TestSet sheets of the Supplementary Data. The conversion rates used for the costings are provided in the Conversions sheet of the Supplementary Data. The hydrocarbon volumes data are provided in Supplementary Table 4.

The CO2 Stored data that support the findings of this study are available from the British Geological Survey and The Crown Estate but restrictions apply to the availability of these data, which were used under license for the current study, and so are not publicly available. Data are however available from http://www.co2stored.co.uk/ after registration which grants a free access. Full data download is considered on a case by case basis by the British Geological Survey and The Crown Estate.

Other data and materials, not specified above, are available from the authors upon reasonable request.

Author contributions statements

JMC co-developed the methodological approach and the models and performed the sensitivity analysis, dataset screening and Monte Carlo simulation. MW conceptualised the study and co-developed the methodology for the screening of the UK dataset and proposed the conceptual design of the idealised store model and provided significant input in the research coordination. DM co-developed the combustor model, and verified the compressor and turbine models, provided the costings of turbine and compressors, and contributed to the development of the predictive models. CMD co-developed the numerical store models in OpenGeoSys. SH contributed to the costing methodology and conceptualised the study. ZS contributed to the conceptual store model development in particular the geomechanical limitations of it. All authors made significant contributions and revisions to the manuscript itself.

Competing Interests

Authors declare no financial and non-financial competing interests.

Figures

Figure 1: Schematic of the key components of a conventional CAES system. At the surface are the plant components, combined with a subsurface porous rock store via a well. The store is charged by using an air compressor. During discharge, the compressed air is fired into a combustion chamber with natural gas and fed into a combustion turbine. The entire work output can be used to generate electricity at a premium retail price, as the air has been pre-compressed during the charging phase.

Figure 2: Workflow to build predictive models of PM-CAES power output and round-trip efficiency and its use to perform a nation scale storage assessment. In step 1 the pressure response induced by cycling air in the store within an idealized aquifer was modelled. In step 2, the outputs from step 1 were corrected using an analytical well model. In step 3, the power consumption and output of compressors and turbines were estimated. In step 4, the outputs from step 3 were used to establish predictive models of the power output and efficiency of the PM-CAES system.

Figure 3: Conceptual model of a well in a porous rock store under PM-CAES operation. No-flow boundaries can be used at the model boundary opposite to the well since the pressure gradients from adjacent wells in a homogenous, isotropic aquifer are assumed to be equivalent in magnitude and in opposite directions.

Impermeable rock layers must be located above and below the porous rock store, so the top and base are also assumed to be no flow boundaries. See Methods for more details.

Figure 4: Map of the United Kingdom showing the formations identified as presenting storage potential in yellow areas. The extent covered by the CO2 Stored dataset is shown in a red outline. Approximate windfarms' location and status is indicated to show the colocation with storage potential.

Figure 5: PM-CAES storage capacity in offshore UK aquifers. The likelihood of achieving a given total storage capacity or less is given by the blue line. This data represents 50,000 iterations of the predictive model applied to the CO2 Stored dataset. The dashed magenta line represents the UK's electricity consumption from the 1st January 2017 to the 28th of February 2017[3]. This line is vertical as a single value is used. This figure shows the variability in storage potential when considering PM-CAES for inter-seasonal storage. It also shows that despite a variability equivalent to 40 % of the UK's winter consumption (based on magenta line) between the 10% likelihood of 77 TWh or less and the 90 % likelihood of 97 TWh or less, there is still enough potential to warrant further investigation.

Tables

Table 1: Criteria for aquifer screening. The information presented here is based on refs 6,23, but also on the insights gained from the modelling (see Justification column).

Parameter	Range/Value	Justification
Depth to the top of the formation	260 - 4000 m	Maximum depth extended for modern compressors and turbines – Minimum depth to prevent well collapse
Permeability	100 - 1330 mD	1330 mD exceeds the recommendation for "excellent" sites, whilst encompassing over 90 % of the database entries.
Thickness	50 - 350 m	Minimum thickness to prevent well collapse
Porosity	15 - 30 %	Within ranges from refs 6,23
Presence of trapping mechanism capable of retaining the stored air near the well	Removed entries for which no known traps or compartmentalisation was identified	Refs 6,23
Lithology	sandstone	Most optimal geology[6] suited to model approximations
Heterogeneity	'complex' geology excluded	Refs 6,23
Overlying seal thickness	> 10 m	Supplementary Table 5.

Table 2: Cost of storage technologies. Batteries are included for comparison, despite not being suited to bulk grid-connected inter-seasonal storage. The levelised costs of electricity presented for PHS, generic underground CAES (which includes the use of salt caverns, mines and porous rocks as stores), and onshore CAES in porous rock, are all applicable to projects with capacities of hundreds of megawatts. The mid-range values reported are taken from literature costing studies when possible, otherwise they are taken as the mean of the low-end and high-end values reported here. The conversion from the original literature value to the US$ 2018 value can be found in Conversions sheet of the Supplementary Data.

Technology	Costs US$ kWh^{-1} (2018)		
	Low-end	High-end	Mid-range
Batteries (NiCd) [9]	0.45	0.63	0.54
PHS	0.11[62 (EPRI)]	0.30[62 (EPRI)]	0.20 (mean)
Generic underground CAES	0.06[62(EPRI-135MW)]	0.25[9]	0.155(mean)
Onshore CAES in porous rocks	0.07[63]	0.13[63]	0.14[64]
Offshore CAES in saline aquifers (this study; see Supplementary Tables 6, 7 and 8)	0.42	4.71	1.48

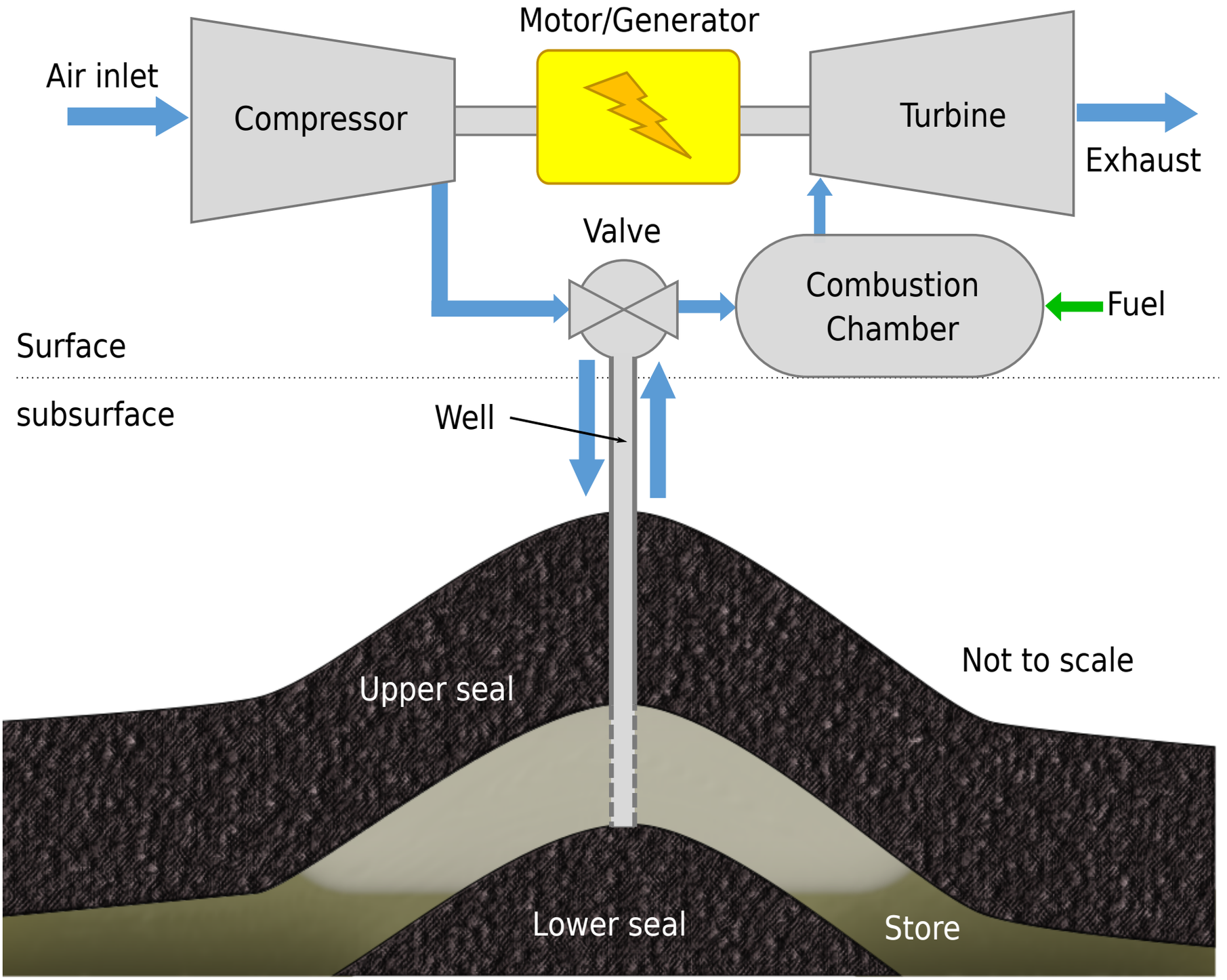
Motor/Generator
Air inlet
Compressor
Turbine
Exhaust
Valve
Combustion Chamber
Fuel
Surface
subsurface
Well
Not to scale
Upper seal
Lower seal
Store

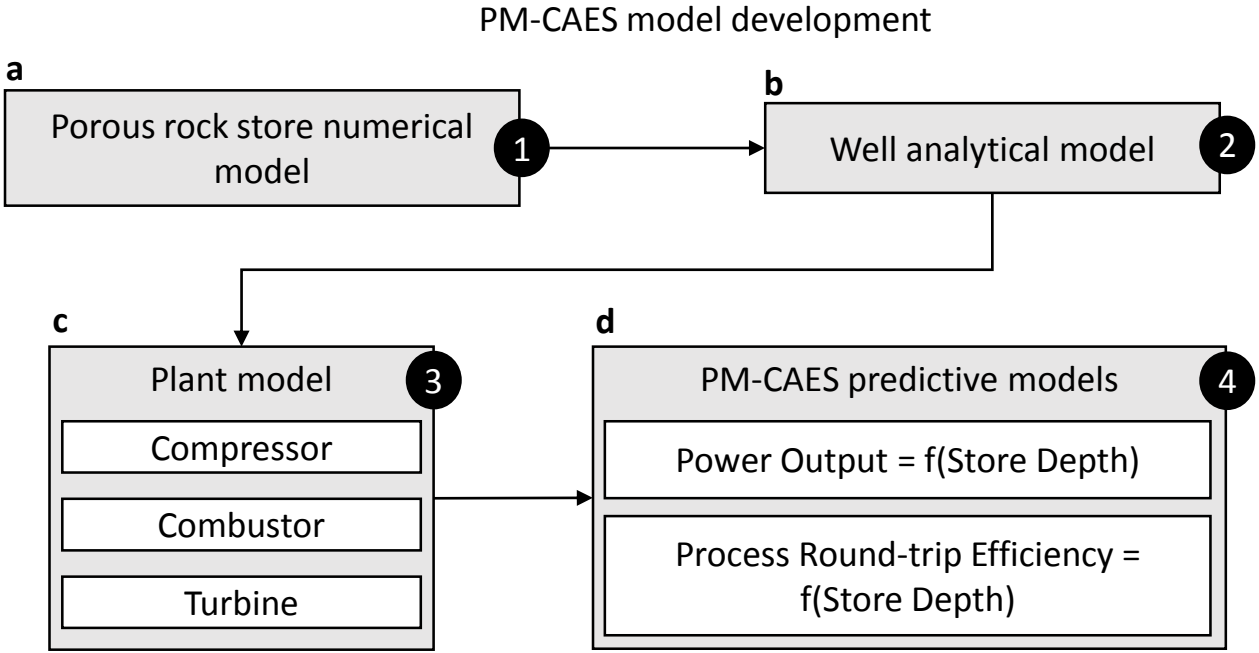
PM-CAES model development
a
Porous rock store numerical model
1
b
Well analytical model
2
c
Plant model
3
Compressor
Combustor
Turbine
d
PM-CAES predictive models
4
Power Output = f(Store Depth)
Process Round-trip Efficiency = f(Store Depth)

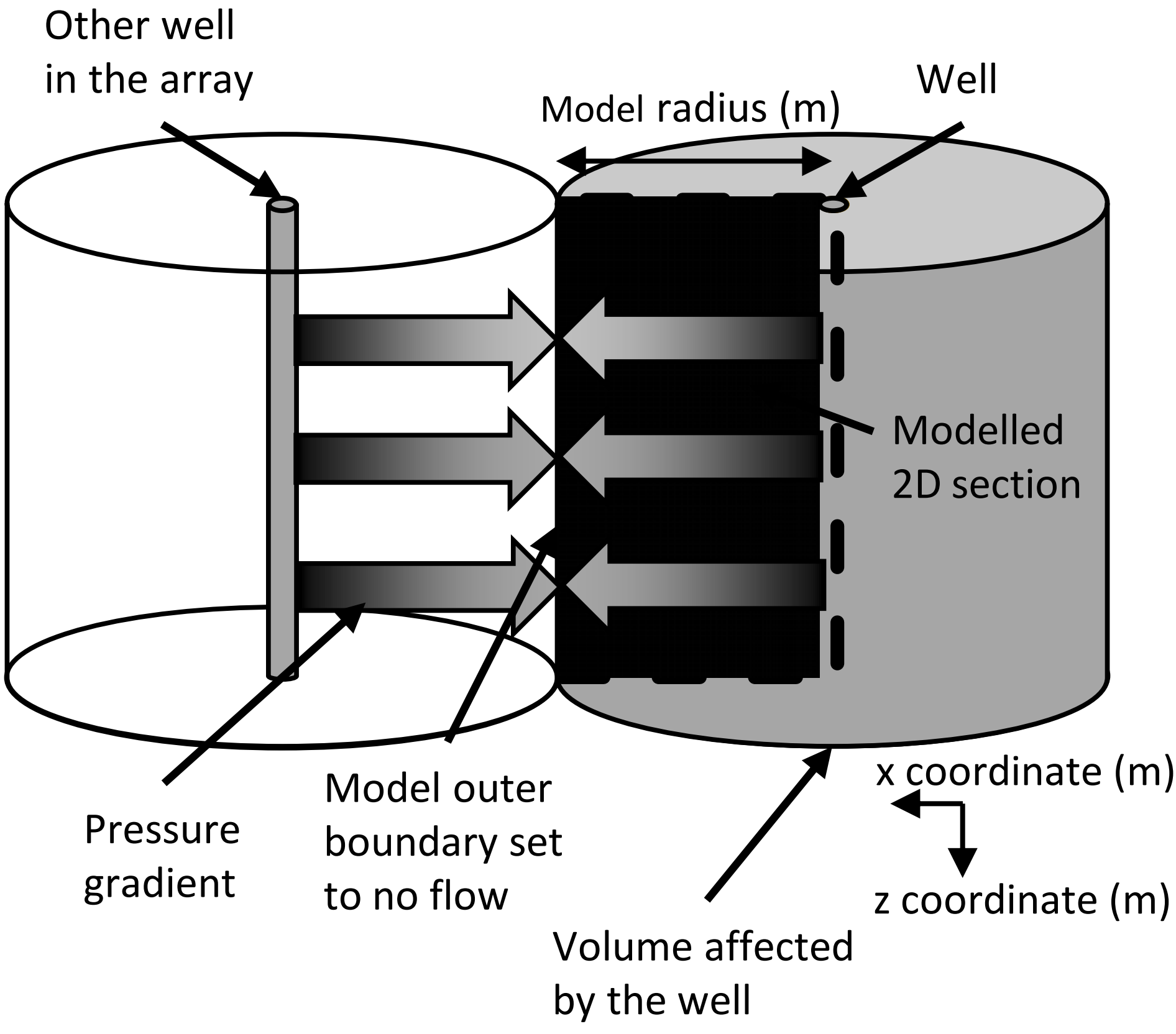
Other well
in the array
Model radius (m)
Well
Modelled
2D section
Pressure
gradient
Model outer
boundary set
to no flow
Volume affected
by the well
x coordinate (m)
z coordinate (m)

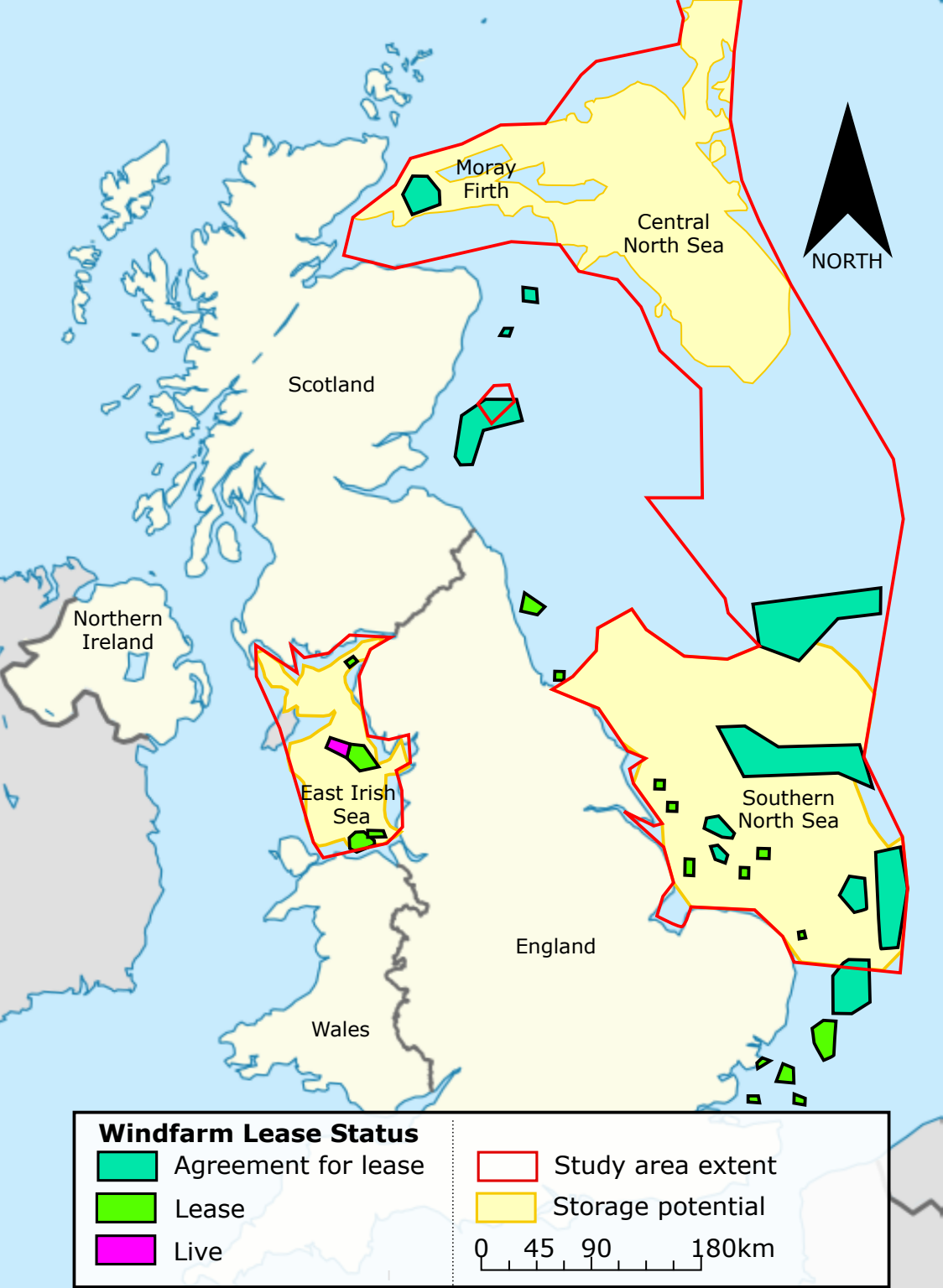
Moray
Firth
Central
North Sea
NORTH
Scotland
Northern
Ireland
East Irish
Sea
Southern
North Sea
England
Wales
Windfarm Lease Status
Agreement for lease
Lease
Live
Study area extent
Storage potential
0 45 90 180km

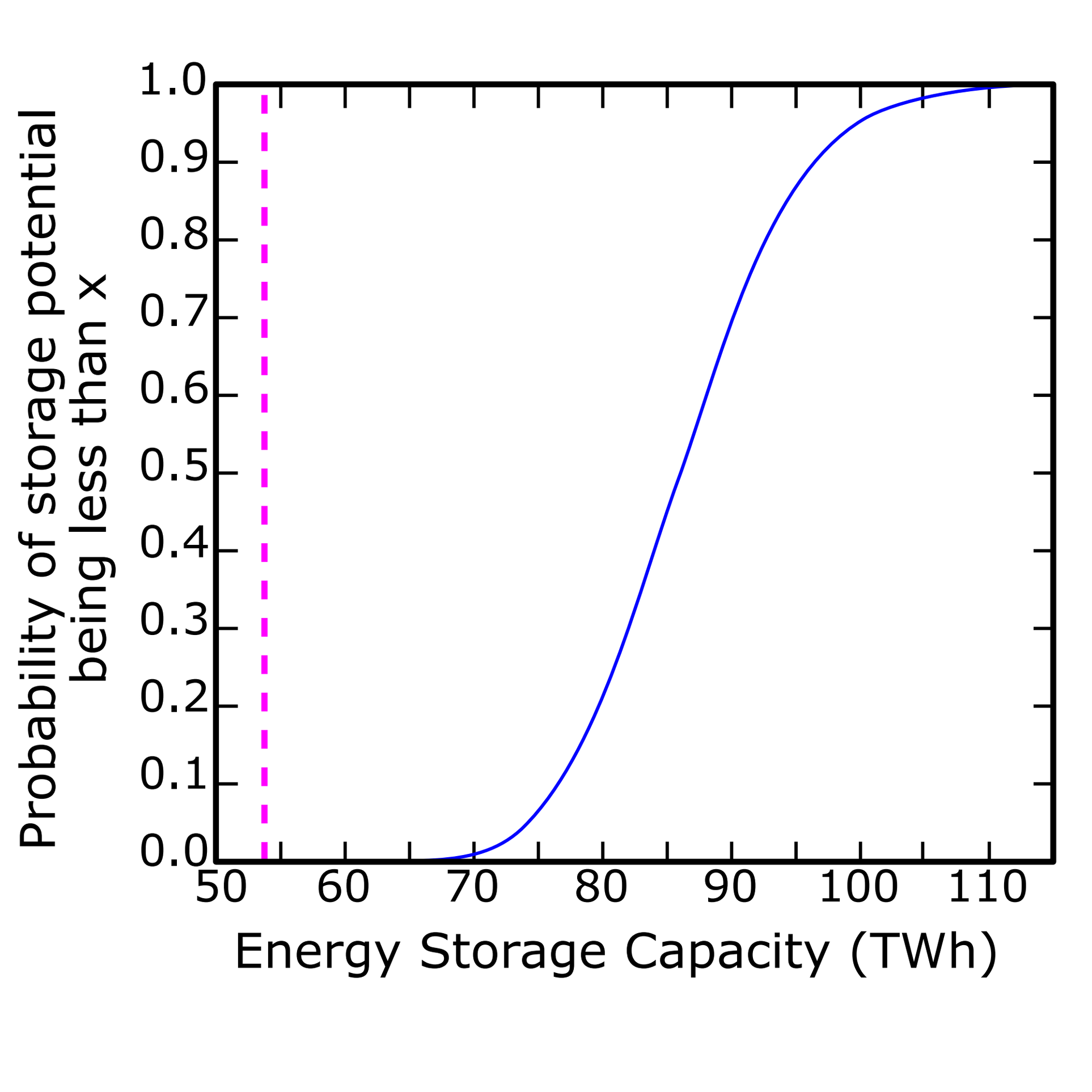
Probability of storage potential being less than x
1.0
0.9
0.8
0.7
0.6
0.5
0.4
0.3
0.2
0.1
0.0
50
60
70
80
90
100
110
Energy Storage Capacity (TWh)

Supplementary Information to article “Inter-seasonal compressed air energy storage using saline aquifers”

Authors: Julien Mouli-Castillo*[a], Mark Wilkinson[a], Dimitri Mignard[b], Christopher McDermott[a], R. Stuart Haszeldine[a], Zoe K. Shipton[c]

[a] Grant Institute, School of GeoSciences, University of Edinburgh, West Mains Road, Edinburgh, EH9 3JW, UK

[b] Institute for Energy Systems, School of Engineering, University of Edinburgh, Mayfield Road, Edinburgh EH9 3DW, UK

[c] Department of Civil & Environmental Engineering, University of Strathclyde, Glasgow, G1 1XJ, UK

*Correspondence: Julien Mouli-Castillo, email: julien.moulicastillo@ed.ac.uk

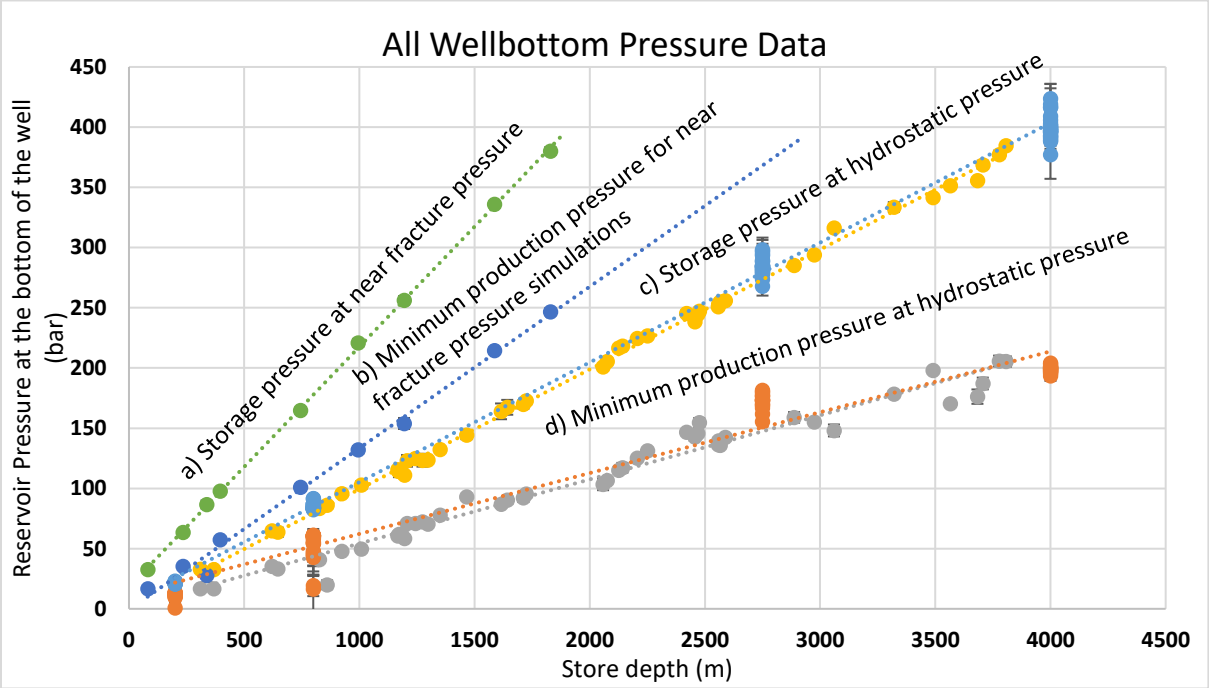

Supplementary Figure 1: Store numerical simulation results. Each line represents the pressure at the bottom of the well. Line a) and c) data was extracted when the store was fully charged. Line b) and d) data was extracted when the store production phase of 60 days had ended. The values plotted represent the average over all the cycles taking place in each simulation, and the error bars the range. Each simulation was allowed 12 hours of computing time. Simulations were filtered to ensure at least 5 of the 10 cycles had been completed within the allotted time (i.e. sample size for each data point).

Supplementary Table 1: Well Power Output Regression Model Summary Statistics

Regression Statistics	
Multiple R	0.995
R Square	0.989
Adjusted R Square	0.989
Standard Error	0.152
Observations	544

ANOVA

	df	*SS*	*MS*	*F*	*Significance F*
Regression	3	1169	390	16715	0.000
Residual	540	13	0		
Total	543	1182			

	Coefficients	*Standard Error*	*t Stat*	*P-value*	*Lower 95%*	*Upper 95%*	*VIF*	*Std. Dev.*
Intercept	-7.3160	0.0949	-77.1304	0.00	-7.5023	-7.1296	NA	NA
Alpha	-1.291	0.0236	-54.607	0.00	-1.337	-1.2450	1.05	0.28
Log10(depth)	3.439	0.0165	207.87	0.00	3.406	3.4717	1.04	0.40
Turbine Polytropic Efficiency	7.790	0.1027	75.841	0.00	7.588	7.9922	1.01	0.06

Supplementary Table 2: Round-Trip Regression Model Summary Statistics

Regression Statistics	
Multiple R	0.976
R Square	0.953
Adjusted R Square	0.9529
Standard Error	1.044
Observations	544

ANOVA

	df	*SS*	*MS*	*F*	*Significance F*
Regression	4	11987.2	2996	2750	0.000
Residual	539	587.3	1.089		
Total	543	12574.6			

	Coefficients	*Standard Error*	*t Stat*	*P-value*	*Lower 95%*	*Upper 95%*	*VIF*	*Std. Dev.*
Intercept	-23.2323	0.82245	-28.2	2.1E-108	-24.847	-21.62	NA	NA
Alpha	-1.0781	0.161156	-6.69	5.6E-11	-1.3947	-0.762	1.04	0.28
Depth^0.5	0.1413	0.002988	47.3	5.2E-194	0.1354	0.147	1.03	15.25
Turbine Polytropic Efficiency	46.4642	0.702408	66.1	7.3E-261	45.084	47.84	1.01	0.06
Compressor Polytropic Efficiency	50.5208	0.773145	65.3	2.6E-258	49.002	52.04	1.00	0.06

Supplementary Table 3: Parameters used to predict wellbore failure analytically. It was assumed that the failure was most likely at the wellbore since that is where the greatest pressure swing will occur. The Poisson ratio, is at the high end of the predicted values for sandstone in order for the result to be conservative[1]. The rock friction angle was taken towards the lower end of the likely encountered angles according to relationships from [2,3]. Lower friction angle lead to a higher threshold for collapse pressure, making this choice a conservative one.

Parameter	Equation / Constants
Cohesive rock strength, τ_0 (Pa)	= 3846.15*depth
Horizontal stress, σ_{max}=σ_{min} (Pa)	= 14519.23*depth
Initial pore pressure, P_0 (Pa)	= 10000.00*depth
Depleted pore pressure, P_0^* (Pa)	= minimum production pressure modelled
Poisson ratio, ν	= 0.25
Rock friction angle, ϕ (°/rad)	= 27/0.47

Supplementary Table 4: Hydrocarbon volumes (V_h) used to estimate the usable storage volumes within aquifer entries of type 2 from the CO2 Stored dataset. OIIP indicates the oil initially in place within the hydrocarbon field, and GIIP the gas initially in place. The formation volume factor and gas expansion factor were used to convert volumes of hydrocarbon at surface pressure and temperature conditions to corresponding volumes at store conditions. The hydrocarbon initial saturation was used to account for pore space occupied by other fluids, usually brine. Highlighted values were taken as averages from all other existing values. For example, 1.4 was the average of all the FVF and 168 that of all the gas expansion factors. For the fields marked with an asterisk the hydrocarbon volume could be found and the GIIP was back-calculated for the sake of completeness.

Aquifer	Field Name	Hydrocarbon Type	OIIP (MMBBL)	GIIP (Billion cu-ft BCF)	FVF / Gas Expansion Factor	Hydrocarbon Initial Saturation	V_h (m3)
Balder	Harding	Oil	322		1.1	0.91	6.35E+07
Balder	West Brae	Oil	116		1.2	0.92	2.33E+07
Balder	Brimmond	Oil	15		1.4	0.7	4.56E+06
Bunter	Main Hewett Lower Bunter	Gas		2100	140	0.80	5.31E+08
Bunter	Main Hewett Upper Bunter	Gas		1356	97	0.78	5.08E+08
Bunter	Gordon	Gas		1843	165	0.78	4.06E+08
Bunter	Esmond*	Gas		1671	158	0.83	3.60E+08
Bunter	Caister B*	Gas		1235	225	0.67	2.32E+08
Bunter	Forbes*	Gas		1116	179	0.84	2.10E+08
Bunter	Orwell	Gas		283	168	0.78	6.11E+07
Bunter	Caister C	Gas		230	285	0.68	3.36E+07
Bunter	Little Dotty	Gas		100	185	0.76	2.01E+07
Burns	Buzzard	Oil	990		1.4	0.78	2.74E+08
Claymore	Claymore	Oil	1453		1.2	0.78	3.49E+08
Forties	Forties	Oil	4196		1.2	0.85	9.57E+08
Forties	Nelson	Oil	790		1.4	0.78	2.19E+08
Forties	Arbroath	Oil	334		1.3	0.55	1.28E+08
Forties	Montrose	Oil	236		1.5	0.55	1.03E+08
Forties	Arkwright	Oil	73		1.5	0.51	3.31E+07
Maureen	Maureen	Oil	398		1.3	0.67	1.22E+08

Maureen	Moira	Oil	12		1.3	0.78	3.17E+06
Maureen	Fleming	Gas		1064	200	0.78	1.93E+08
Mey	Andrew	Oil	4196		1.2	0.85	9.57E+08
Mey	MacCulloch	Oil	200		1.2	0.90	4.24E+07
Mey	Balmoral	Oil	151		1.4	0.78	4.18E+07
Mey	Cyrus	Oil	82		1.4	0.78	2.27E+07
Ormskirk	South Morecambe	Oil	946		1.5	0.75	3.10E+08
Ormskirk	Lennox	Oil	184		1.3	0.78	4.88E+07
Ormskirk	Douglas	Oil	202		1.1	0.78	4.43E+07
Ormskirk	North Morecambe	Gas		5500	143	0.65	1.68E+09
Ormskirk	Hamilton	Gas		627	120	0.78	1.90E+08
Ormskirk	Hamilton North	Gas		230	108	0.78	7.73E+07
Piper	Piper	Oil	1368		1.3	0.95	2.86E+08
Piper	Rob Roy Main	Oil	790		1.4	0.96	1.78E+08
Piper	Rob Roy Supra	Oil	101		1.3	0.94	2.30E+07
Piper	Ivanhoe	Oil	100		1.2	0.91	2.09E+07
Piper	Scott	Oil	42		1.7	0.91	1.23E+07
Piper	Hamish	Oil	7		1.4	0.95	1.70E+06
Piper	Chanter	Gas		95.4	263	0.82	1.25E+07
Piper	Telford	Oil	126		2.2	0.78	5.65E+07
Statfjord	Brent	Oil	3800		1.8	0.78	1.39E+09
Statfjord	Statfjord	Oil	1319		1.5	0.52	5.98E+08
Tor	Banff	Oil	304		1.3	0.78	8.06E+07
Valhall/Wick	Captain	Oil	1000		1.0	0.84	1.98E+08

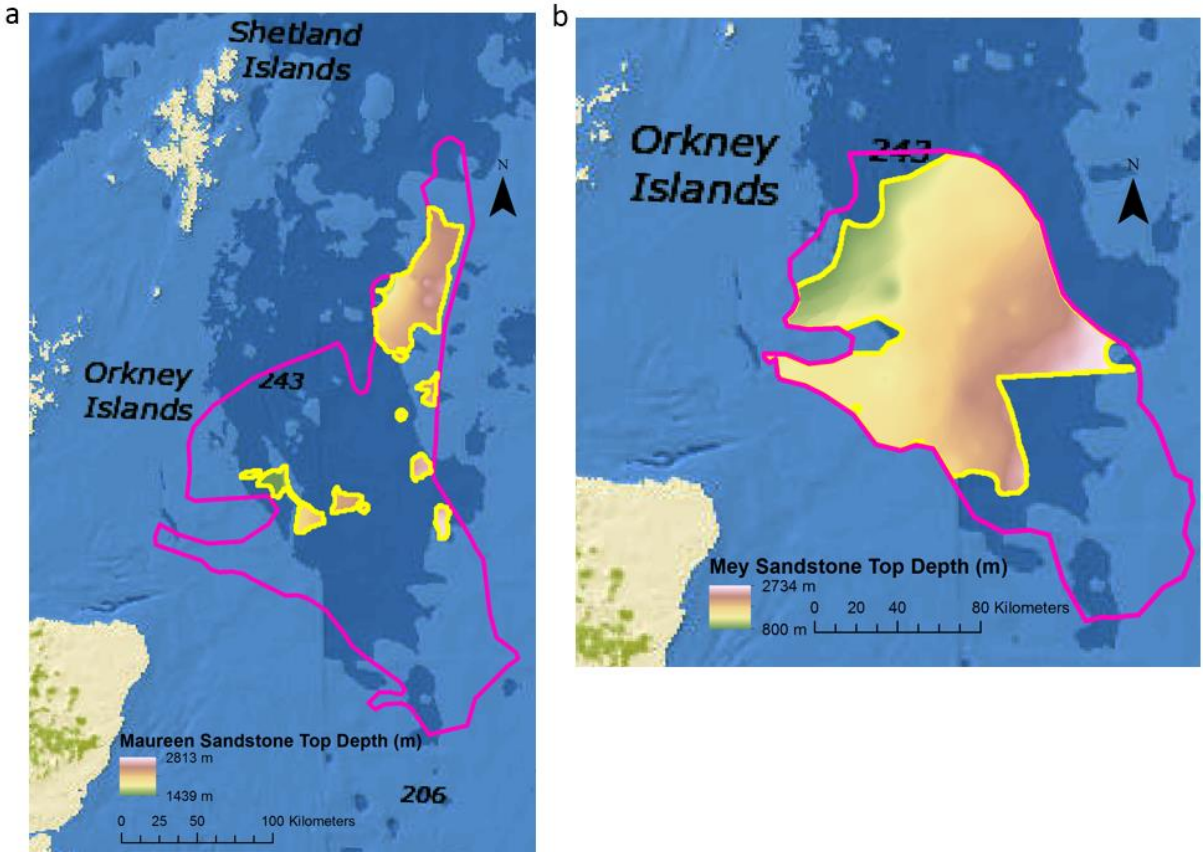

Supplementary Figure 2: Results from the subdivision of two entries of type 1 covering a large areal extend of the North Sea: the Maureen formation (a) and the Mey Sandstone (b). The magenta outline corresponds to the CO2 Stored aquifer extent and the yellow outline to the one used in this study. The Maureen formation was subdivided using, net thickness (Fig. 4.90), porosity (Fig. 4.106), net-to-gross ratio (Fig. 4.94), and permeability (Fig. 4.110) maps from [Main Reference 52], thickness map from [4], as well as 46 well bore correlations from [Main References 49,50] used to generate depth maps using the built-in “inverse distance weighting” tool in ArcMap® , and facies maps (Fig. 10) from [Main Reference 51] from which net-to-gross ratio could be estimated (0.7 in areas of sand thickness of 100s m, 0.35 in sand reach areas of less than ~ 100 m). The sand thickness is correlated to the net-to-gross ratio due to the depositional processes which consists in the addition of sand into a submerged basin, the sand accumulates in thick clean package, whilst the lighter muds remain in suspension for longer and form thinner deposits on the fringes of the massive sand units. The Mey Sandstone was subdivided using net thickness (Fig. 4.22), porosity (Fig. 4.57), net-to-gross ratio (Fig. 4.54), and permeability (Fig. 4.46) maps from [Main Reference 52],as well as 94 well bore correlations from [Main References 49,50], and facies maps (Fig. 10) from [Main Reference 51] from which net-to-gross ratio could be estimated. All filtering was done using the criteria ranges for depth, permeability, thickness and porosity from the Methods Table 2.

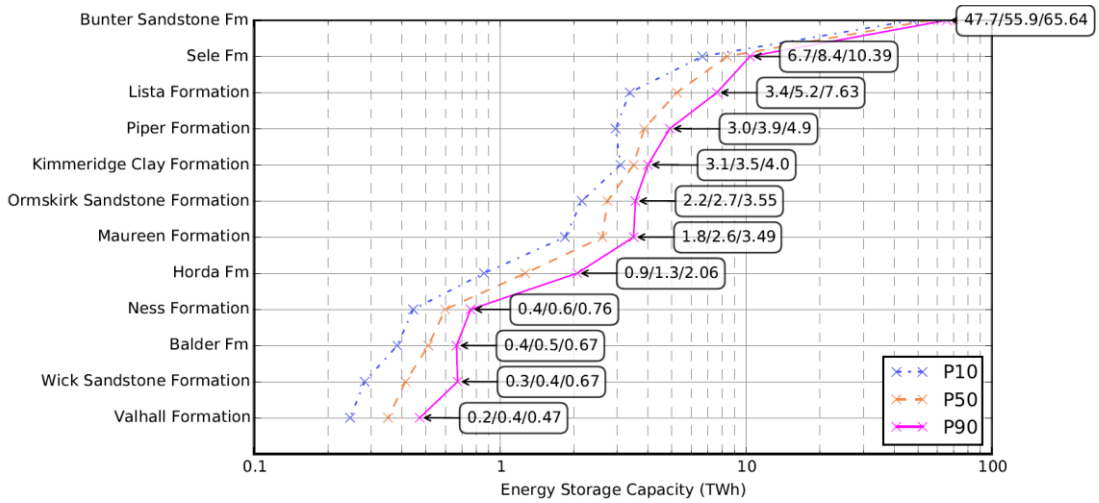

Supplementary Figure 3: Graphical summary of the storage potential estimates per formations where the P10/P50/P90 values correspond to the 10, 50 and 90% likelihood of achieving the stated potential value or less.

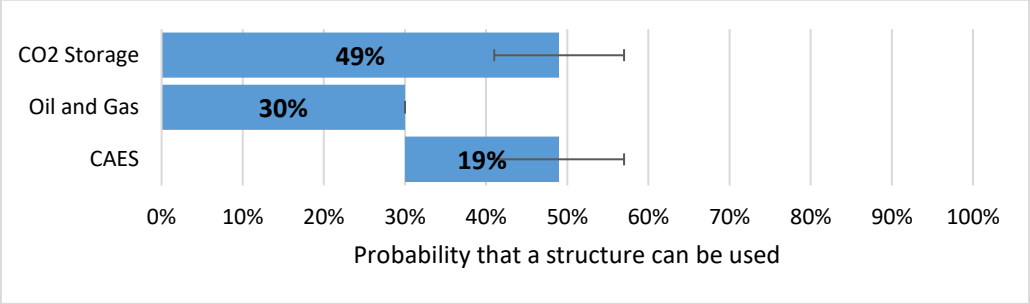

Supplementary Figure 4: Successful exploitation probability for CO2 storage, oil and gas and CAES. The error bars indicate the variation in likelihood of success reported by Xia and Wilkinson for different aquifers using the 90 % confidence interval of a binomial distribution (n = 322)[Main Reference 55].

Supplementary Table 5: Summary of the formations retained in the final PM-CAES storage potential in offshore UK saline aquifers.

Formation Name	Seal Name, Type and Thickness (m)	Energy Storage Potential (50th%ile) TWh	Power Capacity (50th%ile) GW	Share of Storage Potential (%)
Bunter Sandstone Fm.	Dowsing Fm., Rot Mb., Dudgeon Fm., halite and shale > 500[5,6]	55.9	38.2	66%
Sele Fm. (Forties, Cromarty, Flugga, Hermod and Teal Members)	Lista shales > 600 Main Reference 50	8.4	5.7	10%
Lista Fm. (Mey Sst Member).	Lista and Sele shales > 100 Main Reference 50	5.2	3.6	6%
Piper Fm. (Pibroch and Chanter Sst Members)	Kimmeridge Clay shales > 100[7]	3.9	2.6	5%
Kimmeridge Clay Fm. (Burns and Claymore Sst Members)	Kimmeridge Clay and Valhall shales > 100[7]	3.5	2.4	4%
Ormskirk Sandstone Fm.	Mercia Mudstones and evaporites [8]	2.7	1.9	3%
Maureen Fm.	Lista and Sele Shales > 50 Main Reference 50	2.6	1.8	3%
Horda Fm. (Tay Sandstone Member)	Horda Fm. Shales > 100 Main Reference 50	1.3	0.9	1%
Ness Fm.	Heather Fm. Shales > 100 m [7]	0.6	0.4	1%
Balder Fm.	Horda and Balder Shales > 100 Main Reference 47	0.5	0.3	1%
Wick Sandstone Fm. (Punt Member)	Carrack Shales > 50 [9]	0.4	0.3	0%
Valhall Fm. (Scapa Member)	Carrack Shales > 50 [9]	0.4	0.2	0%

Supplementary Table 6: Worst case costing scenario. All costs in 2015 currency.

Inputs			
Site Power Output	40	MW	~ 1 offshore gas turbine
Discount rate, r	0.1	-	High risk
Electricity cost	0.1	£/kWh	about twice the cost reported in ref. 62 (corrected)
Roundtrip efficiency	0.54	-	low end from this study
Distance from shore	250	km	equivalent to the furthest potential storage areas
Well Power	4	MW/well	low end from this study
Well cost	39008323	£/well	Mean value based on ref. 59 + 3 std. dev.
Decommissioning	3E+6	£/well	Maximum value per well from ref. 59 (rounded to nearest million)
Outputs			
LCOE	2.86	£/kWh	
Well number	18		
Energy over lifetime	3.46E+08	kWh	
Costs:			
Wells	6.83E+08		
Turbine Capital	9658304		
Compressor Capital	23861750		
Turbine O&M	3353876		
Compressor O&M	3353876		
Transmission	1.53E+08		
Fuel	15571902		Assumes a natural gas cost of 11.25 £/MMBtu
Charging	45122180		
Decommissioning	52500000		

Supplementary Table 7: Best case costing scenario. All costs in 2015 currency.

Inputs			
Site Power Output	2000	MW	Equivalent to a large windfarm asset
Discount rate, r	0.06	-	Low risk
Electricity cost	0	£/kWh	Free electricity (akin to LCOS from ref. 9)
Roundtrip efficiency	0.59	-	high end from this study
Distance from shore	5	km	near shore
Well Power	11	MW/well	high end from this study
Well cost	10698255	£/well	Mean value based on ref. 59 - 3 std. dev.
Decommissioning	100000	£/well	Minimum value per well from ref. 59
Outputs			
LCOE	0.25	£/kWh	
Well number	318		
Energy over lifetime	2.73E+10	kWh	
Costs:			
Wells	3.4E+09		
Turbine Capital	1.58E+08		
Compressor Capital	1.26E+09		
Turbine O&M	1.83E+08		
Compressor O&M	1.83E+08		
Transmission	4.75E+08		
Fuel	1.23E+09		Assumes a natural gas cost of 11.25 £/MMBtu
Charging	0		
Decommissioning	31818182		

Supplementary Table 8: Mid-range case costing scenario. All costs in 2015 currency.

Inputs			
Site Power Output	1020	MW	Equivalent to a large windfarm asset
Discount rate, r	0.08	-	Low risk
Electricity cost	0.05	£/kWh	Free electricity
Roundtrip efficiency	0.565	-	high end from this study
Distance from shore	127.5	km	near shore
Well Power	7.5	MW/well	high end from this study
Well cost	24853289	£/well	Mean value based on ref. 59 - 3 std. dev.
Decommissioning	1550000	£/well	Minimum value per well from ref. 59
Outputs			
LCOE	0.898	£/kWh	
Well number	223		
Energy over lifetime	8.82E+09	kWh	
Costs:			
Wells	5.55E+09		
Turbine Capital	93213543		
Compressor Capital	6.07E+08		
Turbine O&M	85523842		
Compressor O&M	85523842		
Transmission	2.27E+08		
Fuel	3.97E+08		Assumes a natural gas cost of 11.25 £/MMBtu
Charging	5.39E+08		
Decommissioning	3.46E+08		

Supplementary References

1. Dvorkin, J. P. Can gas sand have a large Poisson's ratio? *Geophysics* **73,** E51–E57 (2008).

2. Chang, C., Zoback, M. D. & Khaksar, A. Empirical relations between rock strength and physical properties in sedimentary rocks. *J. Pet. Sci. Eng.* **51,** 223–237 (2006).

3. Weingarten, J. S. & Perkins, K. Prediction of Sand Production in Gas Wells: Methods and Gulf of Mexico Case Studies. *Soc. Pet. Eng.* 596–600 (1995).

4. Mudge, D. C. Regional controls on Lower Tertiary sandstone distribution in the North Sea and NE Atlantic margin basins. *Tert. Deep. Reserv. North Sea Reserv. North Sea* 403 (2014). doi:10.1144/SP403.5

5. Heinemann, N., Wilkinson, M., Pickup, G. E., Haszeldine, R. S. & Cutler, N. A. CO 2 storage in the offshore UK Bunter Sandstone Formation. *Int. J. Greenh. Gas Control* **6,** 210–219 (2012).

6. Johnson, H., Warrington, G. & Stoker, S. J. Permian and Triassic of the southern North Sea. 6. Lithostratigraphic nomenclature of the UK North Sea. *Lithostratigr. Nomencl. UK North Sea* 1–141 (1994).

7. Richards, P. C., Lott, G. K., Johnson, H., Knox, R. W. O. & Riding, J. B. Jurassic of the Central and Northern North Sea. *Lithostratigr. Nomencl. UK North Sea* 252 (1993).

8. Jackson, D. I. *et al. The geology of the Irish Sea*. *United Kingdom Offshore Regional Report* (1995).

9. Johnson, H. & Lott, G. K. Cretaceous of the Central and Northern North Sea. *Lithostratigr. Nomencl. UK North Sea* 1–206 (1993).